

## AGN FEEDBACK AND GAS MIXING IN THE CORE OF NGC 4636

E. O’SULLIVAN<sup>1</sup>, J. M. VRTILEK<sup>1</sup> AND J. C. KEMPNER<sup>2</sup>

*Draft version September 7, 2018*

### ABSTRACT

*Chandra* observations of NGC 4636 show disturbances in the galaxy X-ray halo, including arm-like high surface brightness features (tentatively identified as AGN driven shocks) and a possible cavity on the west side of the galaxy core. We present *Chandra* and *XMM-Newton* spectral maps of NGC 4636 which confirm the presence of the cavity and show it to be bounded by the arm features. The maps also reveal a  $\sim 15$  kpc wide plume of low temperature, high abundance gas extending 25-30 kpc to the southwest of the galaxy. The cavity appears to be embedded in this plume, and we interpret the structure as being entrained gas drawn out of the galaxy core during previous episodes of AGN activity. The end of the plume is marked by a well defined edge, with significant falls in surface brightness, temperature and abundance, indicating a boundary between galaxy and group/cluster gas. This may be evidence that as well as preventing gas cooling through direct heating, AGN outbursts can produce significant gas mixing, disturbing the temperature structure of the halo and transporting metals out from the galaxy into the surrounding intra-group medium.

*Subject headings:* galaxies: individual: NGC 4636 — galaxies: intergalactic medium — galaxies: halos — X-rays: galaxies

### 1. INTRODUCTION

NGC 4636, the dominant galaxy of a group on the outskirts of the Virgo cluster, is one of the most well-known nearby ellipticals. It is also one of the most X-ray luminous, and has been studied in detail by every major X-ray imaging observatory to date. Spectral imaging with *Einstein* showed the galaxy to be surrounded by an extensive halo of hot gas with a temperature of 0.78-1.21 keV (90% error bounds, Forman et al. 1985). Further studies using *ROSAT* and *ASCA* measured the metal abundance of the gas, found gradients in both the temperature and abundance with radius, and showed the halo to be very extended (Awaki et al. 1994; Trinchieri et al. 1994; Matsushita et al. 1997; Finoguenov & Jones 2000; Buote 2000a; O’Sullivan et al. 2003a). More recently, NGC 4636 has been observed by both *Chandra* and *XMM-Newton*. The initial *Chandra* ACIS-S observation showed unusual structures in the core of the galaxy, most notably “spiral arm” features and a possible ring of high surface brightness emission, thought to be the product of shocks driven by a previous AGN outburst (Jones et al. 2002). Detailed spectral analysis of these data suggests the presence of a cavity in the X-ray halo on the west side of the core (Ohto et al. 2003). Again, AGN activity is the likely cause; plasma from the radio jets of the AGN can displace the gas of the X-ray halo, leaving an apparent void and altering the projected X-ray properties at that point. Analysis of *XMM* RGS spectra shows that there is little or no emission from gas at temperatures below 0.5 keV, and therefore no cooling flow in the system (Xu et al. 2002). NGC 4636 hosts a weak radio source ( $1.4 \times 10^{38}$  erg s<sup>-1</sup>) with small scale jets which account for  $\sim 40\%$  of the radio emission at 1.4 Ghz (Birkinshaw & Davies 1985; Stanger & Warwick 1986). The H $\alpha$  luminosity is measured to be  $2.3 \times 10^{38}$  erg s<sup>-1</sup> (Ho et al. 1997), and an upper limit of  $2.7 \times 10^{38}$  erg s<sup>-1</sup> is estimated for the X-ray emission

of the AGN (Loewenstein et al. 2001).

Using the high quality data available from both *Chandra* and *XMM*, we present spectral maps of the inner galaxy halo of NGC 4636, which reveal interesting temperature and abundance structures. We consider the origin of these structures and their impact on our understanding of galaxy and group halos.

### 2. OBSERVATIONS AND DATA ANALYSIS

NGC 4636 was observed with the *Chandra* ACIS-S (chip S3) for 53 ks on 2000 January 26-27 (ObsID 323) and with *XMM* EPIC for 64 ks on 2001 January 5-6 (ObsID 0111190701). For the *Chandra* observation, the instrument operated in faint mode, and reduction and analysis of the data were performed using CIAO v.3.1 and CALDB v.2.28. Reprocessing, removal of background flares, and creation of responses and background were carried out as described in O’Sullivan & Ponman (2004). Point sources were identified using the WAVDETECT tool. Apart from those in the galaxy core, which were considered false, all were removed.

The *XMM* EPIC instruments were operated in full frame mode with the medium optical filter. The raw data were processed using SAS v.6.0, and reprocessing, filtering for bad pixels and columns and times of high background, and point source removal were performed as described in O’Sullivan et al. (2003b), including use of the ‘(FLAG == 0)’ filter. Background events lists were generated from the Read & Ponman (2003) blank-sky background data, cleaned to match the data. The SAS EVIGWEIGHT task was applied to both source and background events lists, “correcting” the events to account for vignetting. This allows the use of single, on-axis ARF response files for each instrument, which were generated using ARFGEN. Pregenerated RMF files were used, selected by position. The exposure times after cleaning were  $\sim 58.4$  ks for the MOS cameras,  $\sim 50.9$  ks for the PN, and  $\sim 38.9$  ks for ACIS-S.

In order to look for correlations between the structures visible in the X-ray surface brightness images and temperature and abundance changes in the halo, we created spectral maps from the *Chandra* and *XMM* datasets using the method de-

<sup>1</sup> Harvard-Smithsonian Center for Astrophysics, 60 Garden Street, Cambridge, MA 02138, email: eosullivan, jvrtilek@head.cfa.harvard.edu

<sup>2</sup> Dept. of Physics and Astronomy, Bowdoin College, 8800 College Station, Brunswick, ME 04011, email: jkempner@bowdoin.edu

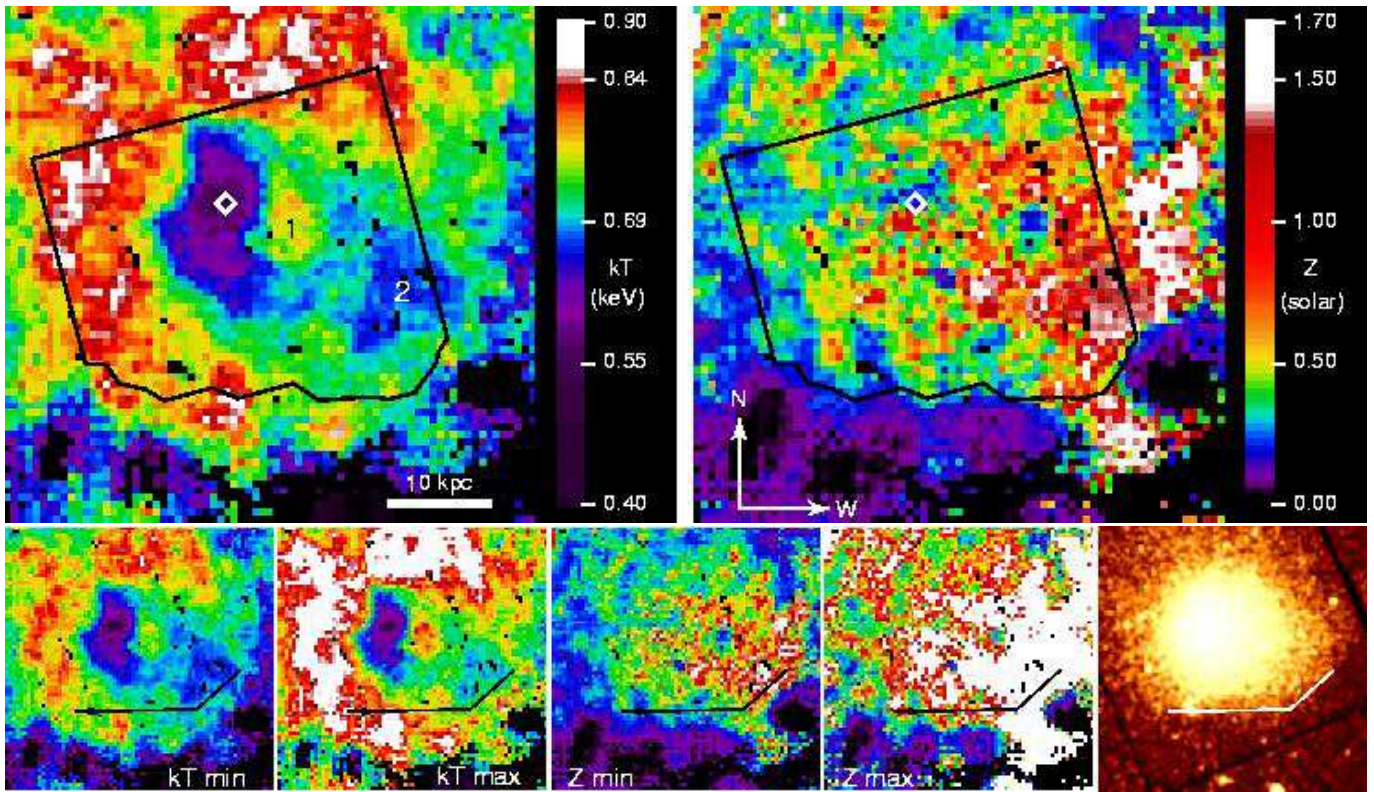


FIG. 1.— *Upper panel:* *XMM* spectral maps of the southwest part of the halo of NGC 4636, showing (*left*) Temperature in keV and (*right*) Abundance in solar units. The maps use  $75 \times 73$   $8.8''^{1/2}$  pixels, whose spectral extraction regions are squares of side  $9-67.5''^{1/2}$ . The diamonds on each map mark the center of the galaxy, regions marked 1 and 2 are, respectively, the cavity and plume referred to in the text. Black lines mark the region of overlap with the *Chandra* spectral maps (see Figure 2). *Lower panel:* Error maps showing the 90% upper and lower limits on temperature and abundance in each pixel, and a gaussian smoothed *MOS 1* surface brightness image of the same field. Lines mark the southern surface brightness edge referred to in the text. 10 kpc is equivalent to  $\sim 130''$ .

scribed in O’Sullivan et al. (2005). The spectra for each map pixel were required to have  $>800$  counts, and were fitted with an absorbed MEKAL model with hydrogen column fixed at the galactic value ( $1.8 \times 10^{20} \text{ cm}^{-2}$ ). Energies below 0.35 (0.5) keV and above 6.0 (8.0) keV were ignored in the *Chandra* (*XMM*) fits. Pixels whose 90% errors on kT were  $>10\%$  (15%) were excluded from the *Chandra* (*XMM*) maps. Figure 1 shows temperature and metal abundance maps generated from the *XMM* data, with associated 90% error maps. For comparison, Figure 2 shows *Chandra* temperature and abundance maps, plotted using the same color scale as used in Figure 1, as well as an X-ray surface brightness image. In each figure, all panels are plotted on the same scale and coordinates, so as to be directly comparable.

Several important features are visible in the temperature maps. Perhaps the most obvious is a region of low temperatures (blue-purple) in the galaxy core and extending in a curve to the south and southwest. To the west of the galaxy core is an area of higher temperatures apparently surrounded by cool gas (region 1 in Figure 1). To the west of this is a large area of moderately cool temperatures (region 2) apparently connected to the core on both sides of region 1. To the north, east, and southeast of the core the temperatures are higher, and this high temperature gas appears to form a boundary around the cool galaxy core and regions 1 and 2, though at the western edge of region 2 it appears to be relatively narrow, with cooler gas beyond. Three main features can be drawn from the abundance maps; first that there is a boundary between high abundance gas in the inner halo, and low abundance gas at the southern and western edges of the maps, with a similar boundary between high and low temperatures; second that the

highest abundances are seen to the southwest of the galaxy core, near region 2 of the temperature map; third, that the abundances in the galaxy core appear to be only  $\sim 0.5$  solar.

Comparing these features to the X-ray surface brightness images we find that the high temperature region 1 seems to be bounded by the western part of the “spiral arm” features. In particular, the southwest “spiral arm” marks the boundary between region 1 and the low temperature curve extending from the galaxy core (see Figure 2). On larger scales the surface brightness appears roughly circular (see Figure 1), but a sharp drop in surface brightness along the south and southwest sides of the inner halo is visible, coincident with the end of region 2 and the southern edge of the area of high abundance. This is probably the boundary between the galaxy halo and a surrounding intra-group or -cluster medium (ICM). Regions 1 and 2 lie roughly along the minor axis of the stellar body of the galaxy. The AGN radio jets do not extend as far as region 1, and are initially aligned  $\sim 43^\circ$  away from the minor axis of the galaxy (Birkinshaw & Davies 1985), but at a small distance from the center they appear to bend, with the southern jet turning to point toward region 1.

There are issues which could affect the absolute accuracy of our maps. Many map pixels will not be independent, due to overlapping spectral extraction regions and the large *XMM* PSF. We have also not corrected for differences in the soft component of the background between the source and background datasets. The fact that both *Chandra* and *XMM* maps show the same features and similar temperatures and abundances at given positions is a strong argument that the PSF issue and background differences are not causing significant problems. It is also important to point out that we are in-



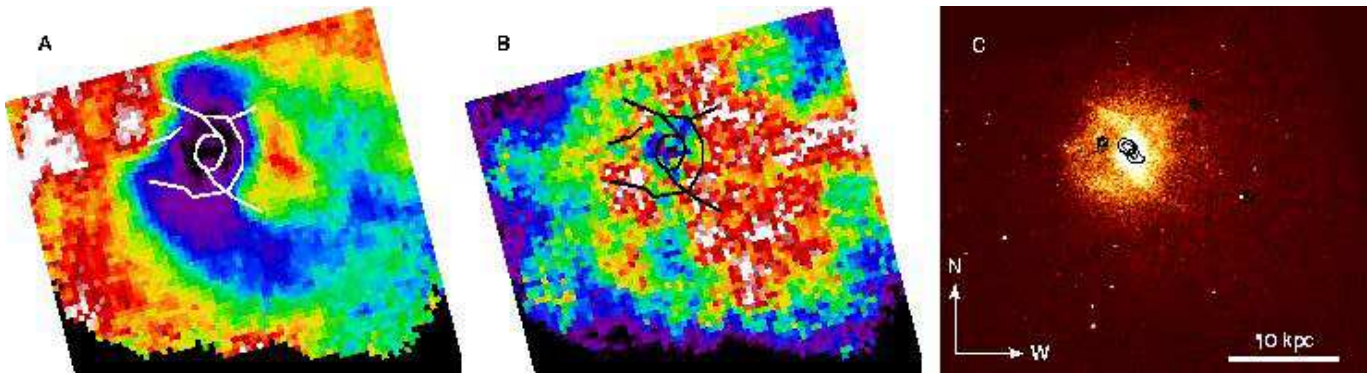


FIG. 2.— *Chandra* temperature (A) and abundance (B) maps of the core of NGC 4636, using the same color scheme as in Fig. 1. The maps use  $64 \times 64 \ 6.4''^2$  pixels, whose spectral extraction regions are squares of side  $8.4 \cdot 63''^{1/2}$ . For comparison, a *Chandra* 0.5-2.0 keV surface brightness (C) image is also shown. All images are on the same scale and centered on the same coordinates. VLA 21cm radio emission contours are overlaid on panel C, and outlines of the surface brightness features are overlaid on panels A and B to aid comparison. 10 kpc is equivalent to  $\sim 130''$ .

interested in relative differences in temperature and abundance across the maps, rather than the absolute value in each pixel. However, as a further test, we carried out more traditional spectral fits for selected regions of the *XMM* data. We extracted spectra from regions centered on the features in the spectral maps and fitted them with a variety of models. With the exception of the galaxy core, all fits produced results in agreement with the maps. The galaxy core required a multi-temperature plasma and power-law model, and while the resulting temperatures agreed with the maps, abundance was a factor  $\sim 2$  higher. The cause is probably the “Fe-bias” effect, the single temperature map fit underestimating the abundance of multi-temperature emission (Buote & Fabian 1998; Buote 2000b). With this exception, we believe these spectral fits show the maps to be an accurate representation of the true temperature and abundance structure.

### 3. DISCUSSION

The high temperatures observed at region 1 correspond closely with the results reported by Ohto et al. (2003), and confirm their suggestion of a cavity in the gas. The apparent curve of the southern radio jet toward region 1 adds further support, and we note that the cavity lies along the minor axis of the galaxy, where the density gradient might be assumed to be steepest. The temperature map suggests that the cavity is non-spherical, and instead has a concave surface toward the galaxy center. This is reminiscent of the bell-like shapes seen in some numerical simulations of buoyantly rising bubbles of radio plasma in galaxy clusters (e.g., Churazov et al. 2001). Given the high temperatures around the north, east, and southeast of the core, it seems likely that the core is surrounded by a spherical shell of hot gas through which a plume of cool gas, ending in region 2, has penetrated. Under this assumption, the high temperature of the cavity is a projection effect, indicating that there is less cool gas along the line of sight than is the case for the surrounding regions.

Taking a simple model of the cavity as a spherical bubble of radio plasma expanding into and rising through the X-ray plasma of the galaxy halo, we can estimate the time taken to create the cavity. Assuming the cavity expands without causing shocks in the halo, we can limit the expansion velocity to the sound speed of the halo gas, leading to an expansion time of  $\sim 23$  Myr. From Churazov et al. (2000), the velocity at which the bubble rises owing to its own buoyancy is  $v_b = C\sqrt{rGM/R^2}$ , where  $R$  is the distance of the bubble from the galaxy core,  $r$  is the radius of the cavity, and  $C$  is a numerical constant for which a value of 0.5 is accepted

for incompressible fluids. This yields a buoyant rise time of  $\sim 47.5$  Myr, but this should be considered a lower limit as this assumes a large difference in gas density between the galaxy core and the current location of the bubble. These two timescales together suggest that the bubble may have formed close to its current location, rather than at the core of the galaxy. We can also estimate the power required to produce the cavity, assuming it expands at the sound speed and the pressure equilibrium between the radio and X-ray plasmas is maintained. From Churazov et al. (2000), the power required is  $Power = 4\pi r^3 KP/3t$  where  $K = (\gamma - 1)/\gamma$ ,  $\gamma$  is the adiabatic index of the relativistic gas in the bubble (i.e.  $\gamma = 4/3$ ),  $t$  is the expansion time of the cavity and  $P$  is the pressure of the halo around the cavity. From this we estimate the power required to be  $\sim 4.8 \times 10^{42}$  erg  $s^{-1}$ . This can be compared to the current luminosity of the core of NGC 4636,  $L_X \simeq 3 \times 10^{41}$  erg  $s^{-1}$  within 20 kpc.

These estimates are considerably higher than the observed X-ray and radio emission of the AGN, but 2-3 orders of magnitude below estimates of the power required to create the larger cavities seen in some galaxy clusters (Böhringer et al. 2002). The radio luminosity to jet power conversion factors of Bicknell et al (1997) suggest that the total current jet power is  $\lesssim 3 \times 10^{41}$  erg  $s^{-1}$  (assuming a magnetic field strength  $> 10^{-4}$  G and the age of the jet to be the bubble expansion timescale), and given the lack of a direct connection between the jets and the cavity, it seems likely that the AGN is currently in a quiescent state, and that the cavity is a remnant of a previous outburst. A similar situation is observed in Abell 4059, which has large cavities in the X-ray halo, but a central radio galaxy whose has declined since their formation (Heinz et al. 2002). There is also the possibility that the AGN outburst was more powerful than our calculations suggest, and caused supersonic expansion of the bubble; the “spiral arm” features in the core were Jones et al. (2002) identified by Jones et al. (2002) as shocks, and a rapidly expanding cavity might shock surrounding gas. However, the resolution of our spectral maps and the size of the spectral extraction regions means that we cannot comment on these features, except to point out their association with the cavity. In any case, the cavity size and power required are small by the standards of galaxy clusters.

One possible reason for this could be that AGN power is related to the mass of the central supermassive black hole (SMBH), so that differences in SMBH mass ( $M_{SMBH}$ ) cause differences in outburst strength and cavity size. Merritt & Ferrarese (2001) estimate  $M_{SMBH} = 7.9 \times 10^7 M_\odot$  for

NGC 4636, based on the stellar velocity dispersion, while van der Marel (1999) calculates  $M_{\text{SMBH}}=3.6 \times 10^8 M_{\odot}$  based on the central optical brightness profile. Estimates for M87 are higher,  $M_{\text{SMBH}}=3.0 \times 10^9 M_{\odot}$  (Tremaine et al. 2002) being typical. This suggests that NGC 4636 has a SMBH  $\sim 5$ -40 times less massive than M87, and if outburst power is directly proportional to  $M_{\text{SMBH}}$ , this might explain the difference in cavity sizes. It is unclear whether there is a general difference in  $M_{\text{SMBH}}$  between group and cluster dominant ellipticals, as only a few measurements are available. However, we note that in the Merritt & Ferrarese (2001) sample, all galaxies with  $M_{\text{SMBH}} > 10^9 M_{\odot}$  are cluster dominant ellipticals, apart from NGC 4649, which is at the center of a subclump of the Virgo cluster. Another point is that galaxy groups (and individual ellipticals) have short cooling times compared to clusters. This implies that the AGN duty cycle in NGC 4636 should be short; after an outburst a cooling flow will be rapidly reestablished and may soon fuel a new outburst. These factors suggest a model in which NGC 4636 produces small outbursts relatively often, while cluster dominant ellipticals produce a smaller number of more powerful events.

Region 2 may be relevant to this argument. The temperature maps suggest that there is a plume of gas extending southwest from the galaxy core, with region 2 forming the tip of the plume and the cavity of region 1 embedded within it. The direction of this plume matches that of the galaxy minor axis. The high abundances to the southwest of the galaxy core suggest that much of the gas in this area has been enriched, and the most likely explanation of this is that the gas was enriched inside the galaxy, then transported outward. In such a model, the plume and cavity can be interpreted as a snapshot of an ongoing series of small AGN outbursts, producing cavities which entrain metal rich, cool gas from the galaxy core. Entrainment of gas by buoyant bubbles is predicted from simulations (Churazov et al. 2000), and high resolution X-ray observations of the radio/X-ray arms of M87 show regions of multi-temperature gas which seem likely to be entrained gas (Molendi 2002). The width of these structures in M87 is  $\sim 8$ -10 kpc, whereas the NGC 4636 plume is  $\sim 15$  kpc across.

If this scenario is correct, the cool plume and high abundances require the AGN of NGC 4636 to have been active prior to the episode which produced the cavity visible in the temperature map, and to have significantly affected the struc-

ture of the galaxy halo. The removal of cool, enriched gas from the galaxy core would clearly affect the formation of any cooling flow, and could have important implications for enrichment in galaxy groups, as it provides a mechanism for the diffusion of metals from the central elliptical into the surrounding intra-group medium (IGM). The sharp drop in X-ray surface brightness, temperature and abundance at the south and west edges of the maps all suggest that this marks the boundary between gas associated with the galaxy, enriched by stellar mass loss and supernovae, and gas associated with a larger potential, which has a much lower metallicity. This surrounding gas could be the halo of the group of which NGC 4636 is the dominant member, or the Virgo ICM. Confirmation of ICM with  $kT \simeq 0.5$  keV and  $0.1$ - $0.2 Z_{\odot}$  abundance at 2.6 Mpc from the cluster core would be an interesting result in itself, but may be unrealistic. Simulations of entrainment by AGN jets in clusters suggest that the mixing effect is not strong enough to affect observed abundance gradients (Brüggen 2002). However, these simulations do suggest that gas can be moved distances of 15-20 kpc, comparable to the motion suggested by our maps. If there is a boundary in NGC 4636 between gas associated with the galaxy and the IGM at a distance of 25-30 kpc, then motions on the scale seen in the simulations would be sufficient to mix the two, particularly if multiple AGN outbursts are considered.

#### 4. CONCLUSIONS

Using X-ray data from *XMM-Newton* and *Chandra*, we have mapped the temperature and metallicity structure of the inner halo of NGC 4636. The maps confirm the presence of a cavity to the west of the galaxy, and show a plume of cool, metal-rich gas extending beyond the cavity to the southwest. Both cavity and plume appear to be the product of past AGN activity, the AGN being quiescent at present. The most likely scenario involves AGN outbursts producing bubble which then entrain enriched gas as they rise buoyantly from the galaxy core. If this is the case, then AGN activity may play an important role in producing both the temperature and abundance structures we observe in galaxy groups.

The authors would like to thank L. David, T. Ponman and C. Jones for useful discussions of this Letter, and an anonymous referee for several helpful comments. Support for this work was provided by NASA grant AR4-5012X.

#### REFERENCES

- Awaki, H., et al. 1994, PASJ, 46, L65  
 Böhringer, H., Matsushita, K., Churazov, E., Ikebe, Y., & Chen, Y. 2002, A&A, 382, 804  
 Bicknell, G. V., Dopita, M. A. & O'Dea, C. P. O. 1997, ApJ, 485, 112  
 Birkinshaw, M., & Davies, R. L. 1985, ApJ, 291, 32  
 Brüggen, M. 2002, ApJ, 571, L13  
 Buote, D., & Fabian, A. 1998, MNRAS, 296, 977  
 Buote, D. A. 2000a, ApJ, 539, 172  
 —. 2000b, MNRAS, 311, 176  
 Churazov, E., Brüggen, M., Kaiser, C. R., Böhringer, H., & Forman, W. 2001, ApJ, 554, 261  
 Churazov, E., Forman, W., Jones, C., & Böhringer, H. 2000, A&A, 356, 788  
 Finoguenov, A., & Jones, C. 2000, ApJ, 539, 603  
 Forman, W., Jones, C., & Tucker, W. 1985, ApJ, 293, 102  
 Heinz, S., Choi, Y., Reynolds, C. S., & Begelman, M. C. 2002, ApJ, 569, L79  
 Ho, L. C., Filippenko, A. V., Sargent, W. L. W., & Peng, C. Y. 1997, ApJS, 112, 391  
 Jones, C., Forman, W., Vikhlinin, A., Markevitch, M., David, L., Warmflash, A., Murray, S., & Nulsen, P. E. J. 2002, ApJ, 567, L115  
 Loewenstein, M., Mushotzky, R. F., Angelini, L., Arnaud, K. A., & Quataert, E. 2001, ApJ, 555, L21  
 Matsushita, K., Makishima, K., Rokutanda, E., Yamasaki, N. Y., & Ohashi, T. 1997, ApJ, 488, L125  
 Merritt, D., & Ferrarese, L. 2001, MNRAS, 320, L30  
 Molendi, S. 2002, ApJ, 580, 815  
 Ohto, A., Kawano, N., & Fukazawa, Y. 2003, PASJ, 55, 819  
 O'Sullivan, E. and Vrtilik, J. M. and Kempner, J. C. and David, L. P. and Houck, J. C. 2005, MNRAS, 357, 1134  
 O'Sullivan, E., & Ponman, T. J. 2004, MNRAS, 354, 935  
 O'Sullivan, E., Ponman, T. J., & Collins, R. S. 2003a, MNRAS, 340, 1375  
 O'Sullivan, E., Vrtilik, J. M., Read, A. M., David, L. P., & Ponman, T. J. 2003b, MNRAS, 346, 525  
 Read, A. M., & Ponman, T. J. 2003, A&A, 409, 395  
 Stanger, V. J., & Warwick, R. S. 1986, MNRAS, 220, 363  
 Tremaine, S., et al. 2002, ApJ, 574, 740  
 Trinchieri, G., Kim, D.-W., Fabbiano, G., & Canizares, C. 1994, ApJ, 428, 555  
 van der Marel, R. P. 1999, AJ, 117, 744  
 Xu, H., et al. 2002, ApJ, 579, 600